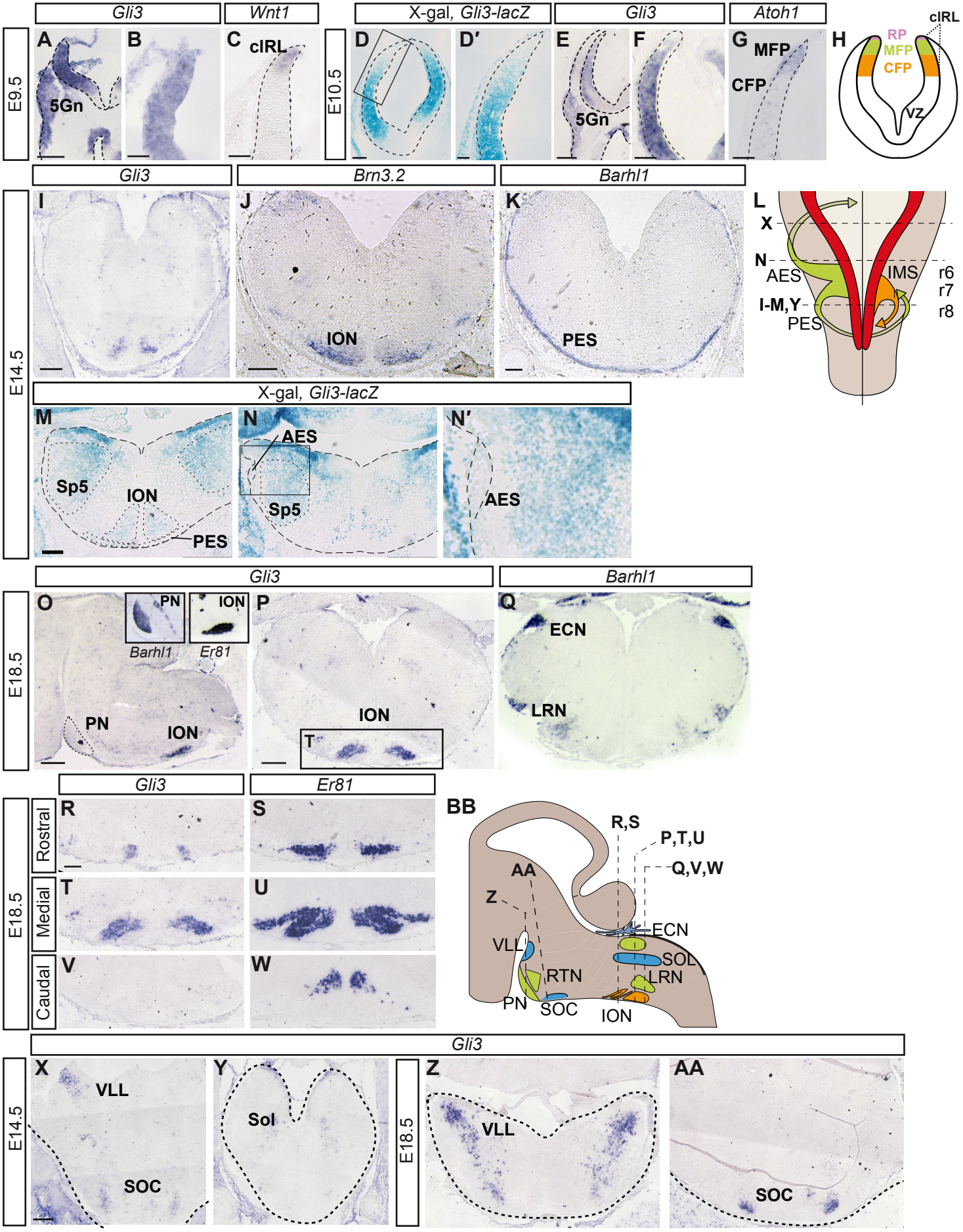

Figure S1: *Gli3* expression in the embryonic hindbrain. (A-C) *In situ* hybridization for *Gli3* and *Wnt1* at E9.5. *Gli3* is expressed throughout the dorsal hindbrain including the *Wnt1*-expressing caudal lower rhombic lib (clRL). *Gli3* is also expressed in the forming trigeminal ganglia (5Gn). n=2 embryos. (D-G) X-gal staining in sections from $Gli3^{lacZ/+}$ embryos and *in situ* hybridization for *Gli3* and *Atoh1*. At E10.5, *Gli3* is no longer expressed in the roof plate (RP) or MF progenitor domain (MFP) but is maintained in the CF progenitor domain (CFP). (D′) Higher magnification of the boxed area in D. n=3 embryos for in situ analysis, n=2 embryos for X-gal analysis. (H) Schematic of the caudal hindbrain at E10.5. VZ: ventricular zone. (I-K) *In situ* hybridization for *Gli3, Brn3.2* and *Barhl1* at E14.5; n=3 embryos. *Gli3* is expressed in a subdomain of the forming ION, but it is not expressed in the PES at E14.5. Rostrocaudal level of sections is indicated in (L). (L) Schematic depicting the precerebellar migratory streams at E14.5. (M,N) X-gal staining in sections from E14.5 $Gli3^{lacZ/+}$ embryos showing expression of lacZ in the spinal trigeminal nucleus (Sp5) and ION. The AES is lacZ negative. (N′) Higher magnification of the boxed area in N. Rostrocaudal level of sections is indicated in (L). n=1 embryo. (O-Q) *In situ* hybridization for *Gli3* and *Barhl1* on E18.5 sagittal sections (O) and coronal sections (P,Q). *Gli3* is expressed in a subdomain of the forming ION, but not in the MF nuclei (PN, LRN, ECN) at E18.5. Rostrocaudal level of coronal sections is indicated in (BB). (R-W) *In situ* hybridization for *Gli3* and *Er81* at E18.5. At E18.5, *Gli3* is expressed in the *Er81*-positive ION subdomain (principal olivary nucleus). (T) Higher magnification of the boxed area in P. Rostrocaudal level of sections are indicated in (BB). (X-AA) *In situ* hybridization on coronal sections for *Gli3* at E14.5 (X,Y) and E18.5 (Z,AA) shows *Gli3* expression in a few specific hindbrain nuclei. VLL: ventral nucleus of the lateral lemniscus, Sol: solitary nucleus, SOC: superior olivary complex. n=3 embryos. Dashed lines outline the tissue. (BB) Schematic depicting the precerebellar nuclei and non-precerebellar *Gli3* expressing nuclei (blue) at E18.5. Scale bars: 50 μm (B,C,D′,F,G); 100 μm (A,D,E); 200 μm (I-K, M-AA).

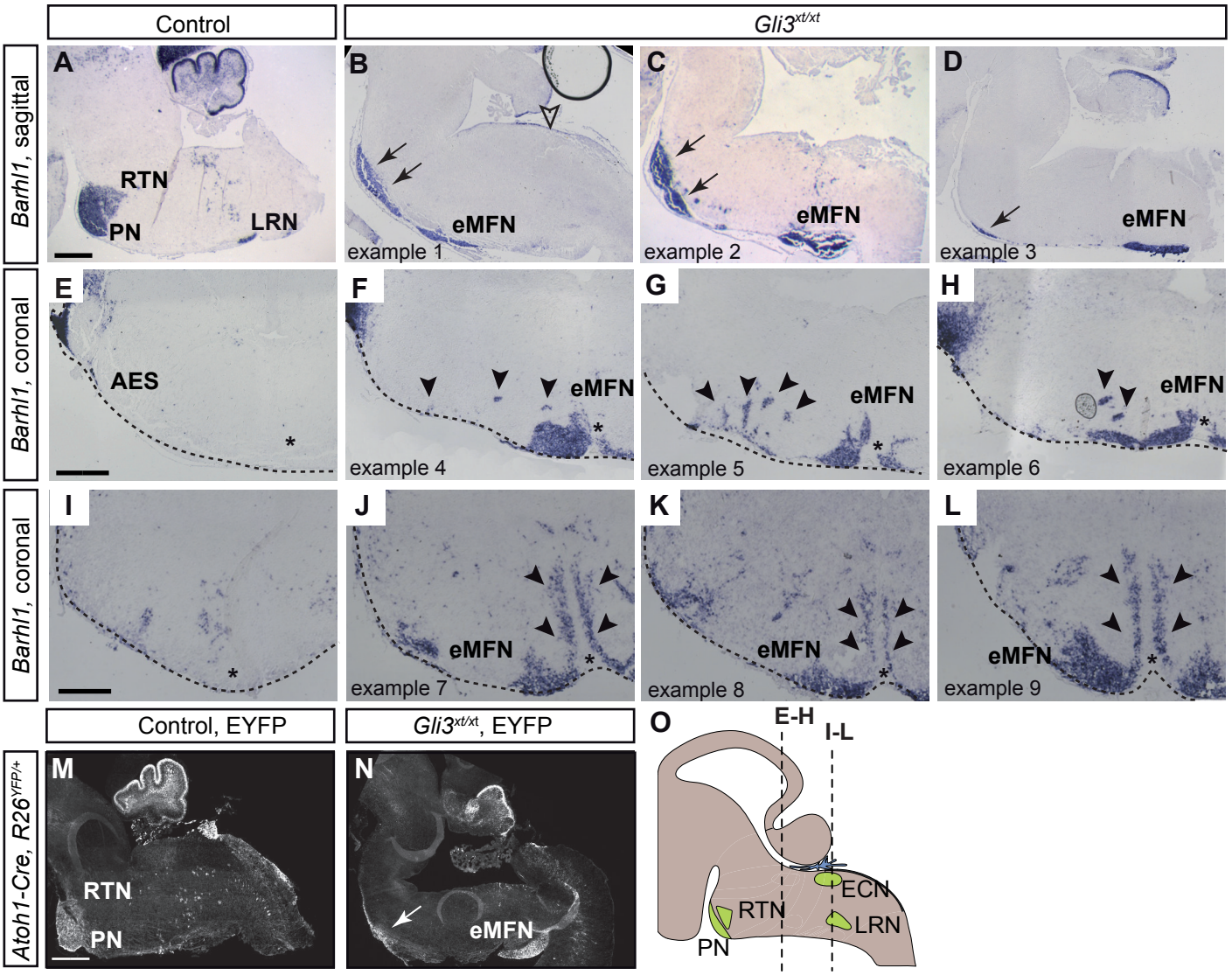

Figure S2: Variable phenotype of MF nuclei in *Gli3*$^{xt/xt}$ mutants. (A-H) *In situ* hybridization for the MFN marker *Barhl1* on sagittal (A-D) and coronal sections (E-L). In some *Gli3*$^{xt/xt}$ mutants, the PN and RTN are partially formed at their normal position in r4 (B-D, arrows). (E-L) *Barhl1*-positive MFN clusters are in ectopic positions (eMFN) along the ventral midline (asterisks) of the hindbrain. In some mutants (n=5/15), there is a strong asymmetry between the nuclei on both sides of the midline. (F-H) eMFN at the ventral midline (asterisks) at the r5/6 level in *Gli3*$^{xt/xt}$ mutants. The presence of small, more laterally located Barhl1-positive cell clusters (arrowheads), suggest that cells delaminate ectopically from the AES in *Gli3*$^{xt/xt}$ mutants. Observed in n=9/15 mutants. (I-L) eMFN at the ventral midline (asterisks) at the r7/8 level in *Gli3*$^{xt/xt}$ mutants. Note the stream of cells on both sides of the midline (arrowheads). (M,N)

Immunostaining for GFP in sagittal sections of E18.5 *Atoh1-Cre; R26*$^{EYFP/+}$ brains. Neurons derived from *Atoh1*-expressing rhombic lip cells form eMFN in *Gli3*$^{xt/xt}$ mutants. Arrow indicates remnants of the PN/RTN. Dashed lines outline the tissue. (O) Schematic of the embryonic hindbrain. Level of sections in E-L are indicated. Scale bars: 400 µm.

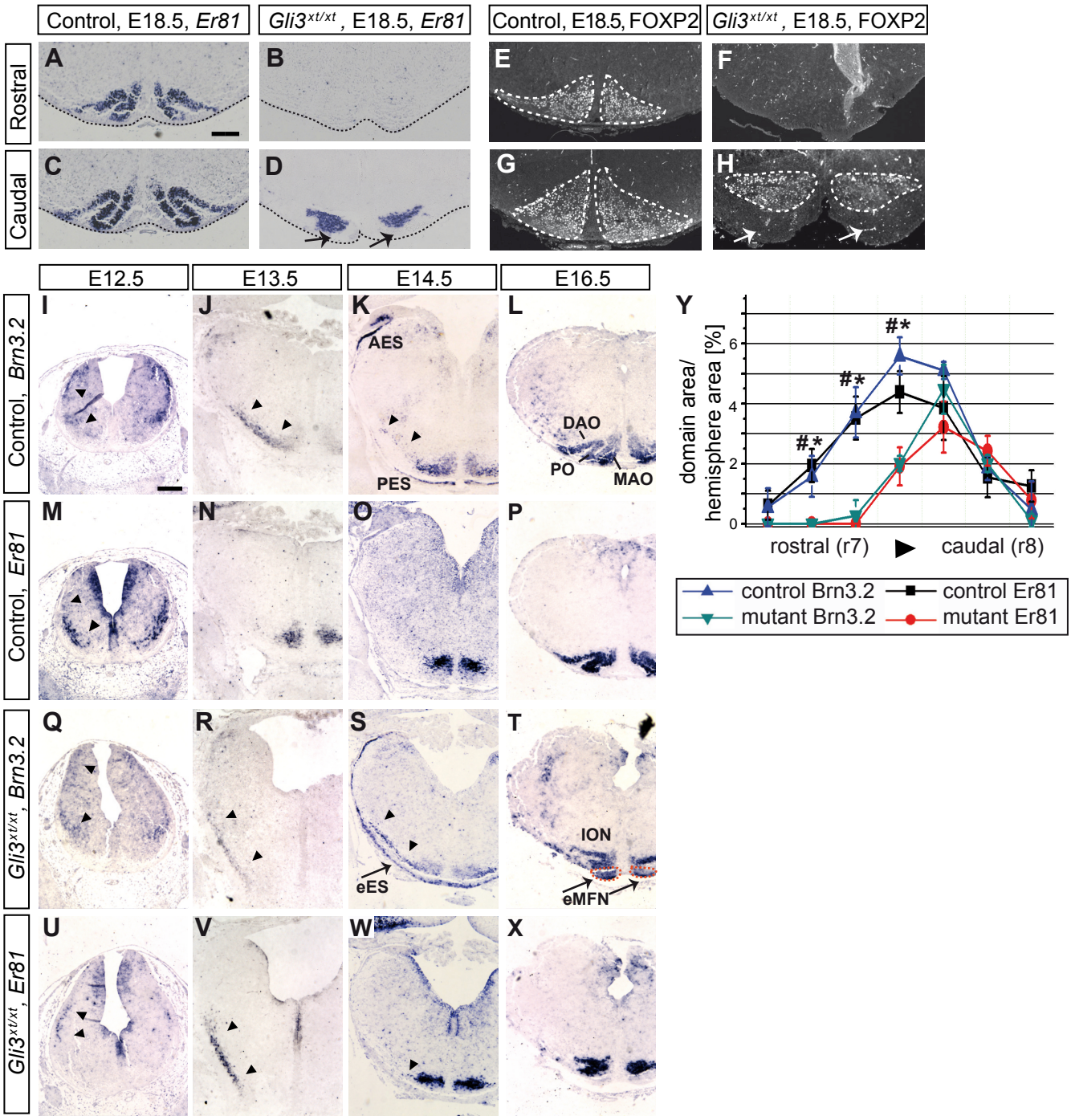

Figure S3: CFN migration and ION formation in *Gli3*$^{xt/xt}$ mutants. (A-H) *In situ* hybridization for *Er81* (A-D) and immunostaining for the ION marker FOXP2 (E-H) on coronal sections at the level of r7/8. The rostral ION is absent in *Gli3*$^{xt/xt}$ mutants and the caudal ION is not organized into the typical layered pattern. Arrows indicate the position of eMFN. 8 control and 8 mutant embryos were analyzed. (I-X) Coronal sections at the level of r7/8 hybridized for *Er81* (I-L, Q-T) or *Brn3.2* (M-P, U-X). *Er81* and *Brn3.2* expression marks different subsets of IMS/ION. *Er81*-positive cells show weak expression of *Brn3.2*. In the control hindbrain, *Er81*-positive cells have reached the ventral midline by E13.5. Arrowheads mark the IMS (I-P). In *Gli3*$^{xt/xt}$ mutants, *Er81*-expressing cells reach the ventral midline only at E14.5. Arrowheads mark the IMS (Q-X). Note that *Brn3.2* is also expressed in the AES and PES in controls (K), in the ectopic extramural stream (eES in S) and ectopic MFN (eMFN in T). By E16.5 the ION has formed in both mutants and controls, but the ION is reduced in size and disorganized in *Gli3*$^{xt/xt}$ mutants as compared to controls. 4 control and 4 mutant embryos were analyzed at E13.5 and E14.5, 2 control and 2 mutant embryos were analyzed at E16.5. (Y) Quantification of the *Brn3.2*- and *Er81*-positive domain along the rostrocaudal extent of the ION in E15.5 coronal sections. Note that the rostral part of the ION is completely absent. The expression area was normalized for the size of the hemisphere at each level and is expressed in percent. Values are represented as mean ± SD. Levene´s test was used to assess equality of variances and an ANOVA one-way with a post-hoc Tukey test was used to test for significance. Hashtag indicates $p<0.05$ for size difference in the *Brn3.2* domain between control and mutant, asterisk indicates $p<0.05$ for the size difference in the *Er81* domain between control and mutant. n=4 brains, for both control and mutant. DAO: dorsal accessory olive, PO: principal olive, MAO: medial accessory olive. Scale bars: 200 µm.

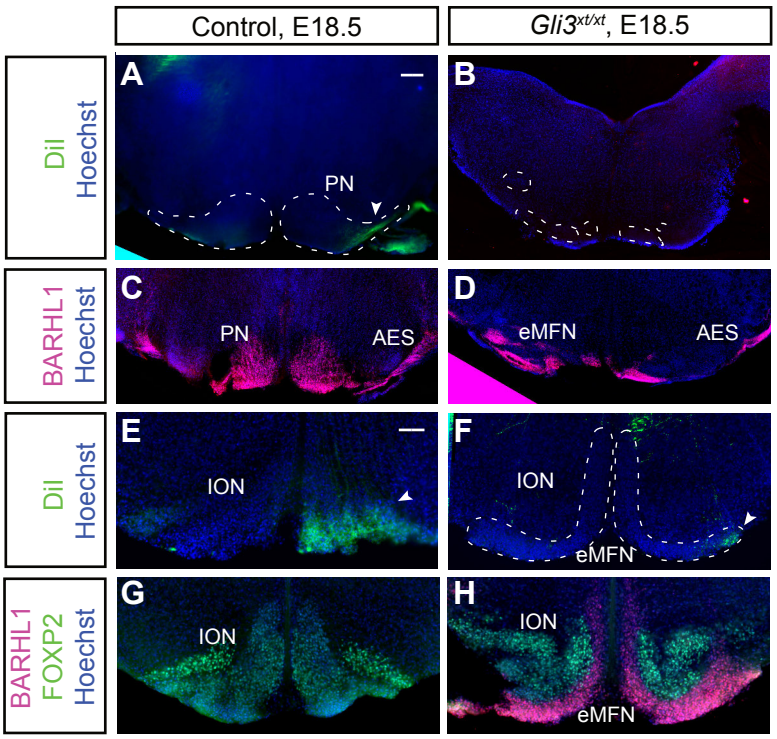

Figure S4: Retrograde tracing of mossy fiber and climbing fiber projections. Hemicerebellar DiI injections to retrogradely label precerebellar nuclei in E18.5 control and *Gli3*$^{xt/xt}$ hindbrains (A, B, E, F). In the control, the contralateral pontine nucleus (PN, r4 in A) and inferior olivary nucleus (ION, r7/8 in E) are strongly labeled with DiI (arrowheads). In the *Gli3*$^{xt/xt}$ hindbrains, ectopic mossy fiber neurons (eMFN) at r5/6 and the ION are negative for DiI (B), though some sparse contralateral eMFN neurons are seen at r7/8 (F, arrowhead). The left side of each image is ipsilateral to the side of DiI injection. Note that the red fluorescent DiI signal was changed to green for better visualization. Adjacent sections show immunostaining for FOXP2 and/or BARHL1 to indicate the position of the ION and MFN (AES, PN and eMFN) (C, D, G, H). 7 controls and 3 mutant embryos were analyzed. Scale bar: 200 µm (A – D), 100 µm (E – H).

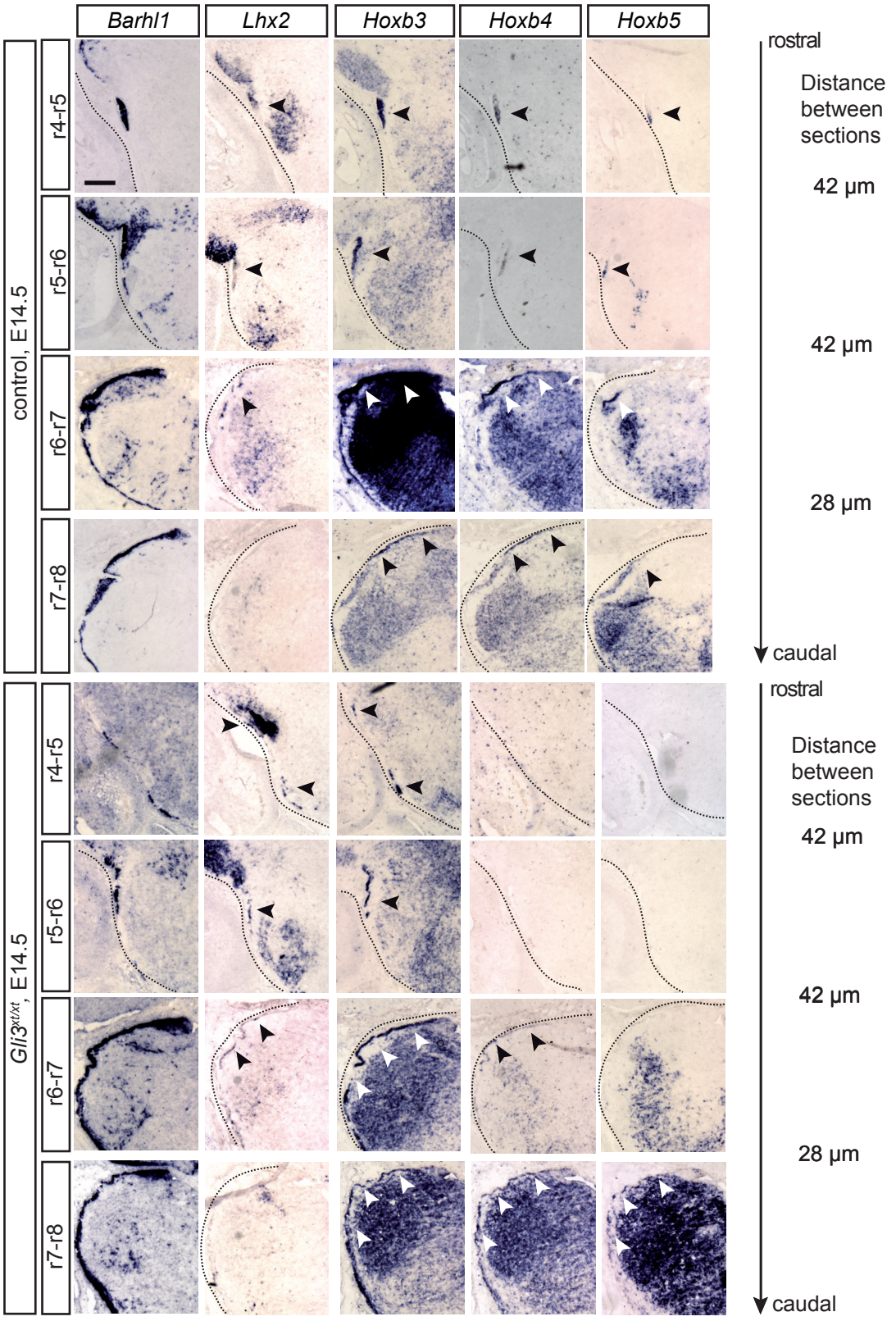

Figure S5: The r7 and r8-derived portion of the AES does not turn rostrally in the hindbrain of *Gli3*$^{xt/xt}$ mutants. *In situ* hybridization for *Barhl1, Lhx2, Hoxb3, Hoxb4* and *Hoxb5* on coronal sections at E14.5. Number of embryos analyzed: 5 controls, 4 mutants for *Lhx2*; 8 controls, 7 mutants for *Hoxb3/4/5*. Arrowheads indicate expression in AES. Scale bars: 200 µm.

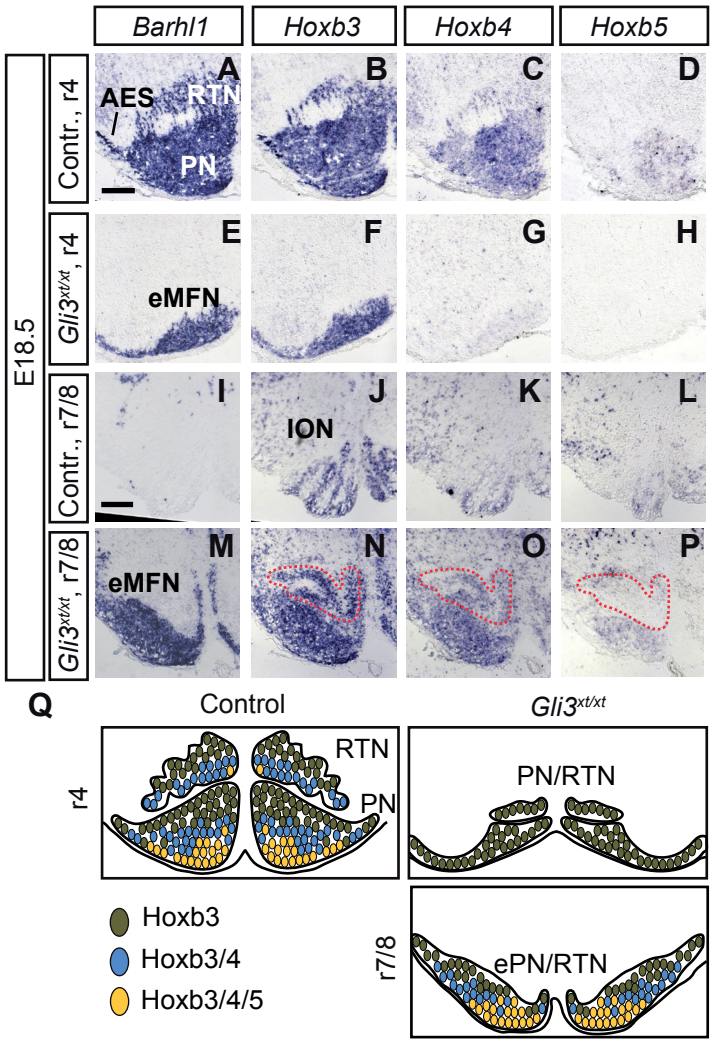

Figure S6: Expression of *Hoxb* genes in the PN/RTN and ION at E18.5. *In situ* hybridization for *Barhl1, Hoxb3, Hoxb4* and *Hoxb5* on coronal sections in r4 and r7/8. Note that the images of *Barhl1*-expressing nuclei are also shown in Figure 2 but are added here for easier comparison (A, E, I, M). In controls, the RTN and rostrodorsal PN expresses *Hoxb3*, the intermediate PN expresses *Hoxb3* and *Hoxb4* and the caudoventral PN expresses *Hoxb3, Hoxb4* and *Hoxb5* (A-D). In *Gli3*$^{xt/xt}$ mutants, the PN forming at the r4-r6 levels is negative for *Hoxb4* and *Hoxb5* (E-H) while the ectopic PN at the r7/8 level expresses all three *Hox* genes (M-P), in a pattern that resembles the Hox expression pattern of the PN in controls. All three Hox genes are also expressed in the ION in controls and *Gli3*$^{xt/xt}$ mutants (I-P, ION outlined with dotted red line in N-P). (Q) Schematic summarizing the *Hoxb* expression patterns in the PN/RTN in control and *Gli3*$^{xt/xt}$ mutants. Number of embryos analyzed: 3 controls, 4 mutants. Scale bars: 200 µm.

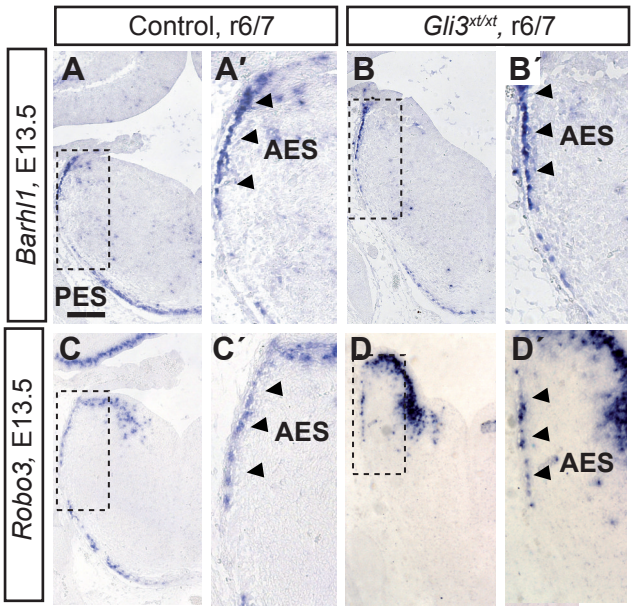

Figure S7: Expression of *Robo3* in the E13.5 hindbrain in controls and *Gli3*$^{xt/xt}$ embryos. *In situ* hybridization for *Barhl1* and *Robo3* on coronal sections. (A′-D′) Higher magnification of the boxed areas in A-D. *Robo3* is expressed in the AES in controls and *Gli3*$^{xt/xt}$ mutants. Number of embryos analyzed: 3 controls, 3 mutants. Scale bar: 200 μm (A-D).

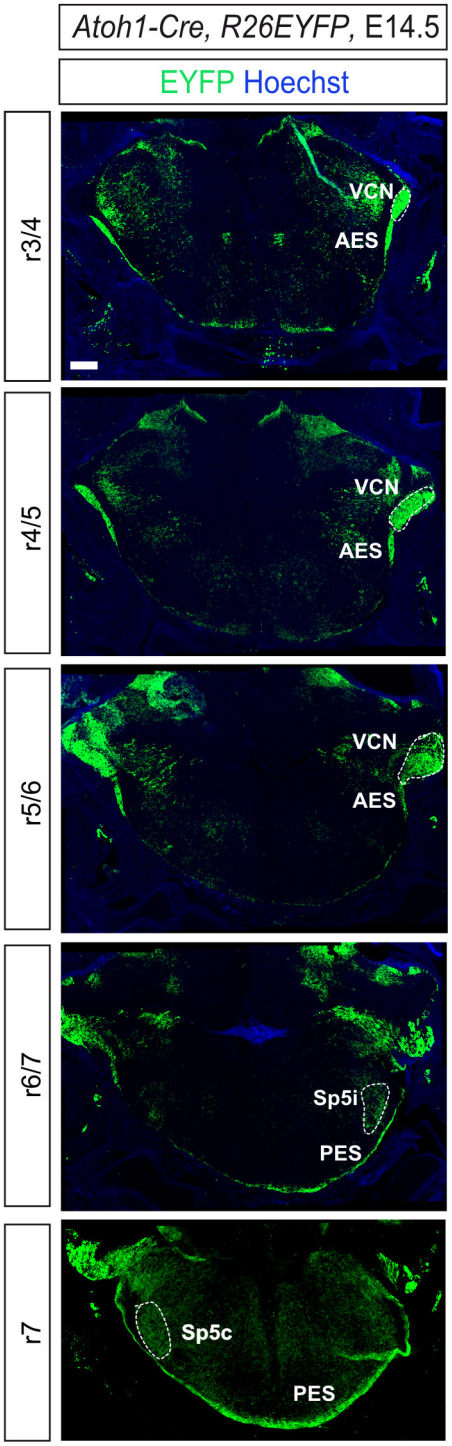

Figure S8: *Atoh1-Cre* induced recombination pattern in the E14.5 hindbrain of control embryos (Genotype: *Atho1-Cre, R26*$^{EYFP/+}$). Immunostaining for EYFP on coronal sections, rostrocaudal levels are indicated. AES, PES, and ventral cochlear nucleus (VCN) are derived from the *Atoh1*-lineage. The *Atoh1*-lineage also contributes neurons to the intermediate and caudal spinal trigeminal nucleus (Sp5i and Sp5c). n=4 embryos. Scale bar: 200 µm.

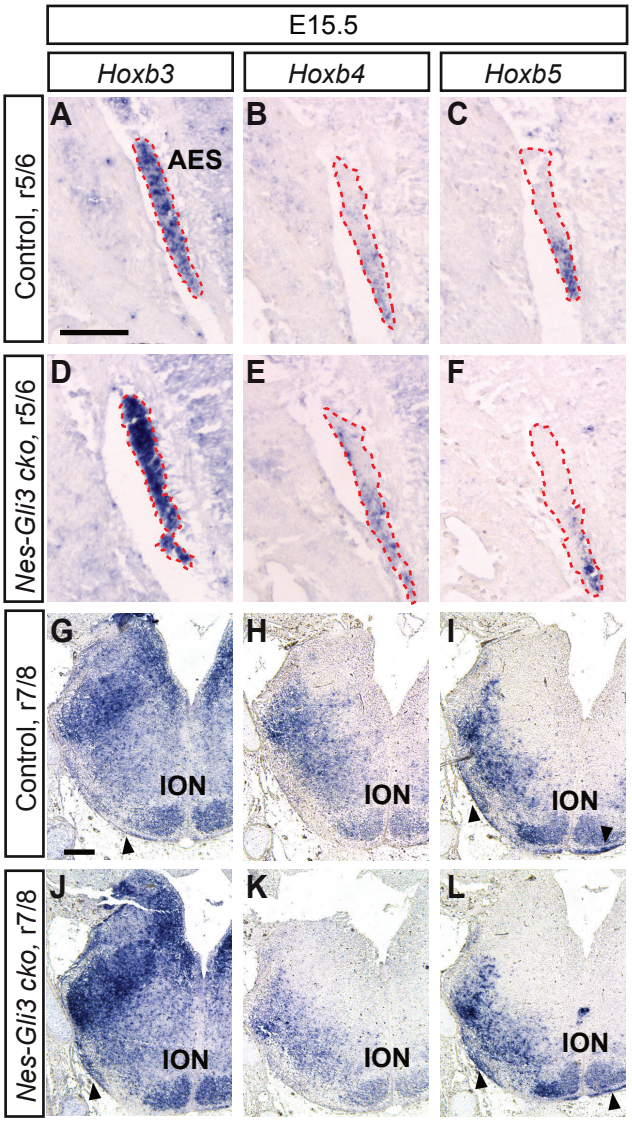

Figure S9: *Hoxb* gene expression is not altered in AES, PES and ION in *Nes-Gli3 cko* embryos. *In situ* hybridization for *Hoxb3, Hoxb4* and *Hoxb5* on E15.5 coronal sections. (A-F) AES is outlined with red dotted line. (G-L) Arrowheads indicate PES. Number of embryos analyzed: 3 controls, 3 mutants. Scale bars: 100 μm (A-F); 200 μm (G-L).

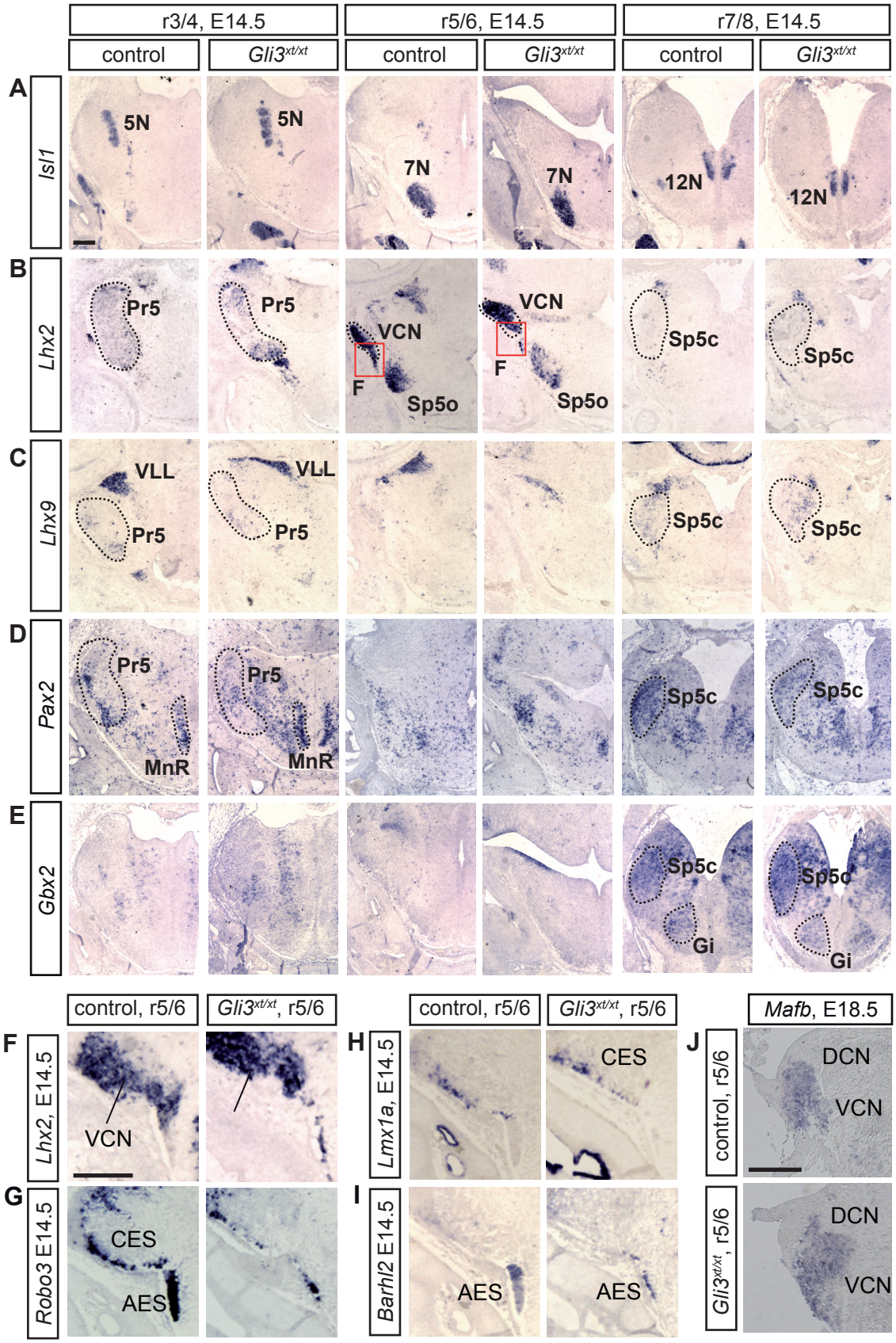

Figure S10: Analysis of non-precerebellar hindbrain nuclei in *Gli3*$^{xt/xt}$ mutants. Coronal sections of control and mutant hindbrain at the level of r3/4; r5/6 and r7/8 hybridized for various *RNA in situ* probes, as indicated. (A) *In situ* hybridization for *Isl1* showing that the motor nuclei of the cranial nerves are present in *Gli3*$^{xt/xt}$ mutants. 8 control and 8 mutant embryos were analyzed. (B) *Lhx2* is expressed in the principal sensory trigeminal nucleus (Pr5) and the oral divisions of the spinal trigeminal nucleus (Sp5o) and the ventral cochlear nucleus (VCN) in control and mutant hindbrain. 5 control and 4 mutant embryos were analyzed. (C) *Lhx9* is expressed in the Pr5, the ventral lateral lemniscus (VLL) and in the caudal division of the Sp5 (Sp5c) in control and mutant hindbrain. 2 control and 2 mutant embryos were analyzed. (D) *Pax2* is expressed in the Pr5, median raphe nucleus (MnR) and Sp5c in control and mutant hindbrain. 3 control and 3 mutant embryos were analyzed. (E) The expression pattern of *Gbx2* in the Sp5c and gigantocellular reticular nucleus (Gi) is comparable in in control and mutant hindbrain. 2 control and 2 mutant embryos were analyzed. (F-K) The cochlear extramural stream (CES, *Robo3* and *Lmx1a* positive in G and H, respectively) and VCN (*Lhx2* and *Mafb* positive in F and J, respectively) in the *Gli3*$^{xt/xt}$ hindbrain are comparable to the CES and VCN in controls. The *Barhl2* positive AES (I) is clearly separated from the CES (G,H) in both control and mutant hindbrain and the VCN is comparable to controls (J). 5 control and 4 mutant embryos were analyzed for *Lhx2* and *Barhl2*; 3 controls and 3 mutants for *Robo3*; 4 controls and 4 mutants for *Lmx1a*; 3 controls and 3 mutants for *Mafb*. 5N, motor trigeminal nucleus; 7N, facial nucleus; 12N, hypoglossal nucleus. Scale bar: 200 μm.

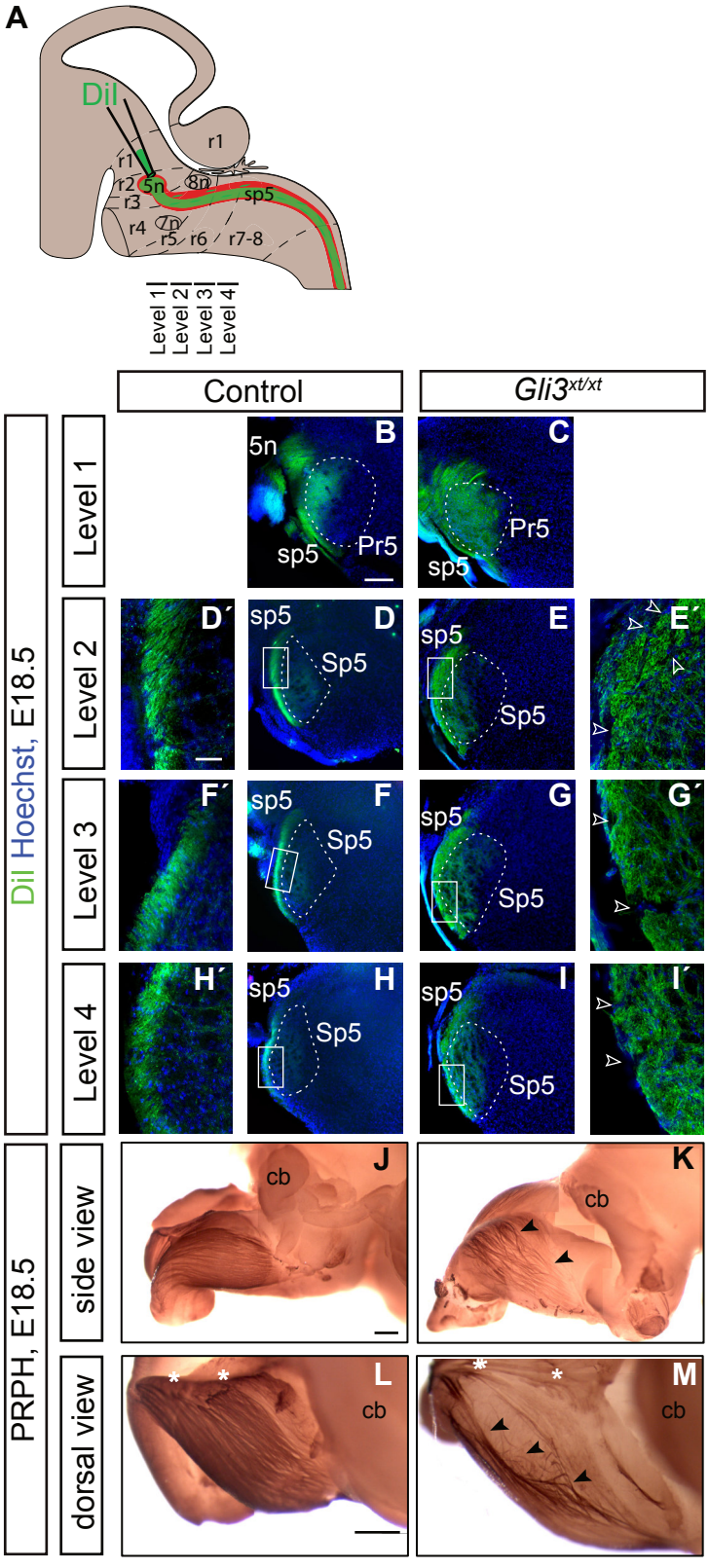

Figure S11: Disorganization of the spinal trigeminal tract in *Gli3*$^{xt/xt}$ mutants. (A-I) Anterograde tracing of central trigeminal projections by injecting DiI into the trigeminal ganglia (5Gn) of E18.5 control and *Gli3*$^{xt/xt}$ mutants. (A) DiI diffusion results in labeling of ascending tract axons innervating the principal trigeminal nucleus (Pr5) and of descending projections forming the spinal trigeminal tract (sp5), which innervate the spinal trigeminal nucleus (Sp5). The rostrocaudal levels shown in B-I are indicated. (B-I) In the control, the sp5 tract is a compact axonal bundle that sends projections into the barrelette neurons of the Pr5 (B) and Sp5 nuclei (D, F, H). In the *Gli3*$^{xt/xt}$ mutants the sp5 tract is defasciculated (arrowheads in E′,G′,I′) and the projections into the barrelettes of the Pr5 and Sp5 are disorganized (C, E, G, I). D′ - I′ are maximum intensity projections of Z-stacks acquired with structured illumination; areas are indicated in D-I. Note that the red fluorescent DiI signal was changed to green for better visualization. n=8 controls, n=2 *Gli3*$^{xt/xt}$ mutants. (J-M) Whole-mount immunostaining for peripherin (PRPH) to visualize the trigeminal tract shows the disorganization of the tract in *Gli3*$^{xt/xt}$ mutants. Side view (J,K) and dorsal view (L,M). Asterisks indicate the dorsal midline. Note that the images are composed of several stitched images to have the entire hindbrain in focus. n=4 controls, n=2 mutants. Scale bars: 200 µm (B-M), 50 µm (D′-I′).

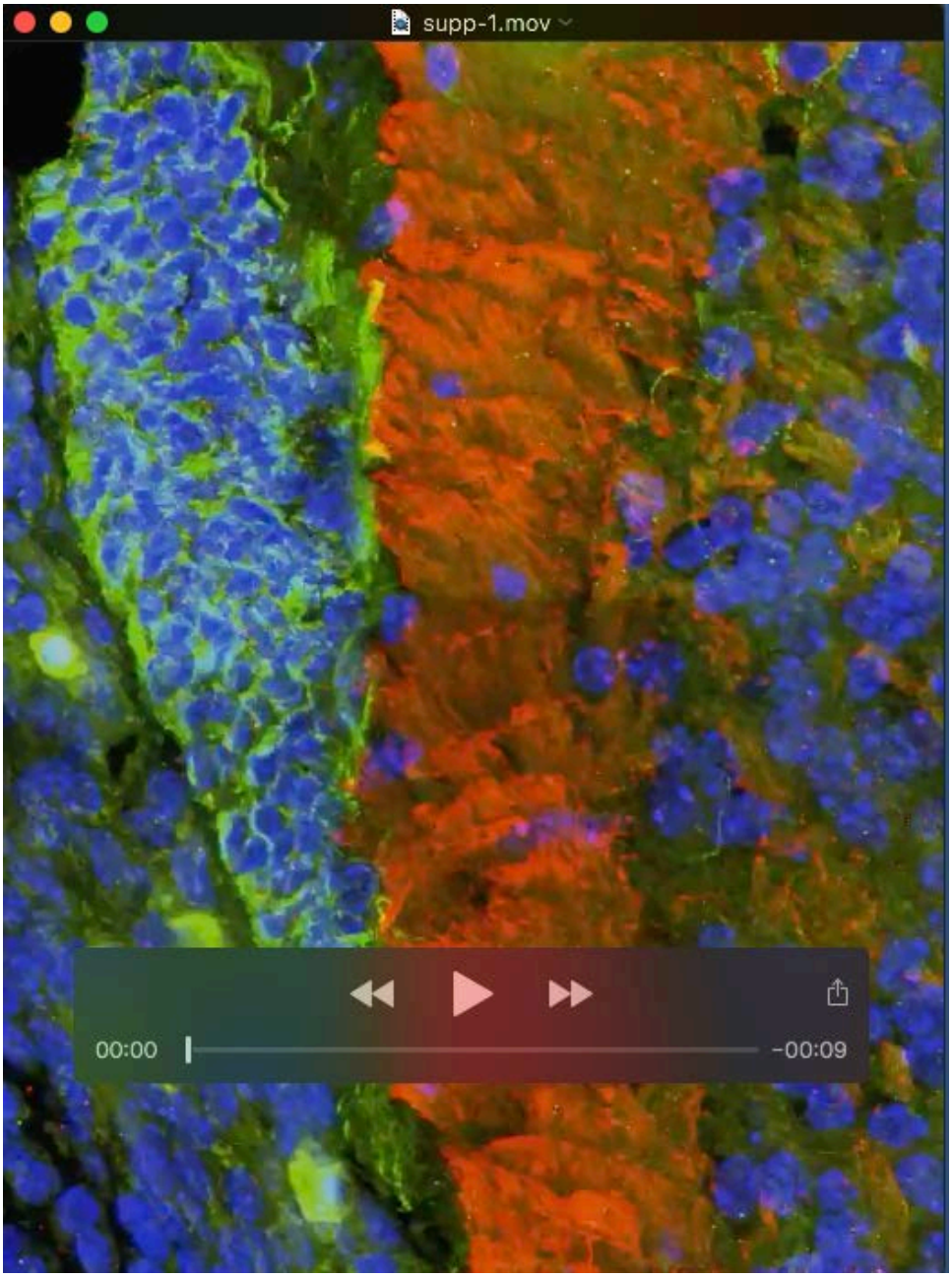

Movie 1: Ventral AES cells are in close contact with the sp5. 3-D projection of a Z-stack of the image shown in Figure 8 K2. Immunostaining for PRPH (red) and DCC (green). Hoechst is in blue. Z-stack was acquired with structured illumination.